ELSEVIER

Journal of Wind Engineering
and Industrial Aerodynamics 96 (2008) 1895–1911

JOURNAL OF wind engineering AND industrial aerodynamics

www.elsevier.com/locate/jweia

Prediction of aerodynamic characteristics of a box girder bridge section using the LES turbulence model

M.W. Sarwar[a,*], T. Ishihara[a], K. Shimada[b], Y. Yamasaki[c], T. Ikeda[d]

[a]*Institute of Engineering Innovation, School of Engineering, The University of Tokyo, 2-11-16, Yayoi, Bunkyo-ku, Tokyo 113-8656, Japan*

[b]*Institute of Technology, Shimizu Corporation, 3-4-17, Etchujima, Koto-ku, Tokyo, Japan*

[c]*Bridge and Road Construction Division, Ishikawajima-Harima Heavy Industry Co. Ltd., 2-2-1 Otemachi, Chiyoda-ku, Tokyo, Japan*

[d]*International Division, Chodai Co. Ltd., 20-4, 1-Chome, Nihonbashi-kakigaracho, Chuo-ku, Tokyo, Japan*

Available online 18 April 2008

Abstract

In this study, aerodynamic characteristics of a box girder bridge section are investigated by three-dimensional computational fluid dynamics using the LES turbulence model. Flow around the streamline box girder section is analyzed, and the effect of section details on the aerodynamic characteristics of bridge section is evaluated. In addition, forced vibration cases are simulated to investigate the aeroelastic behavior of rectangular sections with a high aspect ratio. The flutter characteristics of a box girder bridge section ($B/D = 11.6$) are investigated and compared with experimental results of the generic rectangular cross-sections. Finally, influence of the geometrical modifications on the aeroelastic instability of the bridge section is pursued.

Keywords: LES; Aerodynamic coefficients; Flutter analysis; Box girder bridge section; Section attachments; Computational fluid dynamics

1. Introduction

The safe design of large civil engineering structures like cable-stayed bridges requires investigations on the dynamic response under unsteady wind loads. In this respect,

*Corresponding author. Tel.: +81 35 841 1145; fax: +81 35 841 1147.
E-mail address: sarwar@bridge.t.u-tokyo.ac.jp (M.W. Sarwar).

0167-6105/$ - see front matter © 2008 Elsevier Ltd. All rights reserved.
doi:10.1016/j.jweia.2008.02.015

aeroelastic instabilities of rectangular prisms, because of their common use in bridge industry, have received particular interest from both academic and practical standpoints. Rectangular prisms have quite unique aerodynamic characteristics in the present context; boundary layers separating from the sharp edges may remain separated or have intermittent attachment to the surface of the prism depending on the aspect ratio. Matsumoto (1996) and Matsumoto et al. (1994, 1996) have conducted detailed experimental investigations to understand the aeroelastic characteristics of a rectangular section with a high aspect ratio. This study introduced step-by-step analysis that has shown the predominance of A_1^*, A_2^* and H_3^* on flutter characteristics. Recently, the κ-ε model was employed for the flutter analysis of rectangular sections of varying width to depth ratio by Shimada et al. (2002). However, this study resulted in conservative prediction of the critical flutter velocity for elongated sections, i.e., $B/D = 10$ and 20.

The above mentioned analysis examples are examinations concerning flat rectangular sections assuming that there are no section attachments, e.g., handrails, etc. However, it is general in the field of bridge engineering that many modifications are done to the basic rectangular shapes for obtaining aerodynamically stable cross-sections, e.g., introduction of fairings or for operational purposes like handrails, central barrier, etc. Recently, many studies have shown the use of CFD for predicting the steady and unsteady aerodynamic characteristics of bridge sections. For example, Larsen and Walther (1998) have reported the applicability the of two-dimensional discrete vortex method to predict the flutter characteristics of some generic configuration at first and then extended it to some practical bridge cross-sections. However, this study has resulted in conservative prediction of the flutter critical velocity. Further, Larsen (2006) has reported computation of the aerodynamic derivatives of the box girder section by various 3D CFD techniques. The predicted critical velocity was reported to be sufficiently accurate for LES and DES; however, use of the κ-ω model resulted in underestimation of the critical flutter velocity by 18%.

Though the actual bridge sections include small attachments like handrails, central barrier, etc. previous works have neglected the presence of such details. Therefore, lack of modeling such small details limits the extent of reliability of numerical works that are of much interest from the engineering point of view. Such section details, no matter how small in size compared with the size of the bridge section, can dramatically affect the aerodynamic characteristics of the bridge section not only by controlling the separation point of shear layers but also by changing the flow characteristics around the bridge section (Jones et al., 1995). In addition, Bruno et al. (1998) investigated the effect of section details on the aerodynamic instability of bridge deck using the κ-ε model. Investigations were carried out to investigate the effect of each detail in the absence of others, as well as on the overall behavior in the presence of all details. Even minor changes made to the cross-sectional geometry by safety barriers or sidewalks have shown strong influence on the flow pattern not only in the vicinity of these attachments but also on the section characteristics as a whole. Therefore, it seems necessary at this point to clarify the influence of such details on the overall aerodynamic behavior of the bridge sections.

Recently, Ishihara et al. (2006a) have reported the successful prediction of the flow field around the square prism circumference by LES. Not only the mean pressure coefficient (C_p) but also the fluctuating component of pressure coefficient ($\grave{C}_p$) were reproduced that agreed well with the experimental measurements. The simulation accuracy was further examined by performing an unsteady analysis for a real bridge section under construction,

and has shown the influence of section attachments such as handrails, etc. on the steady aerodynamic coefficients (Ishihara et al., 2006b).

In this paper, the analysis accuracy of the LES model for the real bridge cross-section with section details is investigated. The steady aerodynamic characteristics of the box girder section are obtained by employing the LES model and the effect of small section details, e.g., hand rails, inspection rails, etc., on these characteristics are examined, and comparison with wind tunnel experiments is presented. In addition, forced vibration analysis is conducted following Matsumoto et al. (1994) to investigate the flutter characteristics of the box girder bridge section, and the aerodynamic instability of the box girder bridge section with reference to the rectangular sections of similar width to depth ratio is presented. Further, influence of the geometrical modifications on the aeroelastic instability of the bridge section is summarized. Based on numerical results, application of the LES model to the prediction of flutter critical velocity is discussed.

2. Numerical approach

The LES turbulence model is used in this study in which small eddies are modeled where as large eddies are directly calculated. The finite volume method was used for the discretization of governing equations. Central difference scheme for convective terms and the second-order implicit scheme for unsteady terms were used. The SIMPLEC method was used to solve the discretized equations. The oscillation of the simulation models is achieved by employing the sliding mesh technique. FLUENT (2005) CFD software is used as solver.

2.1. Governing equations

The governing equations employed for LES are obtained by filtering the time-dependent Navier–Stokes equations as follows:

$$\frac{\partial \rho \bar{u}_i}{\partial x_i} = 0, \frac{\partial}{\partial t}(\rho \bar{u}_i) + \frac{\partial}{\partial x_j}(\rho \bar{u}_i \bar{u}_j) = \frac{\partial}{\partial x_j}\left(\mu \frac{\partial \bar{u}_i}{\partial x_j}\right) - \frac{\partial \bar{p}}{\partial x_i} - \frac{\partial \tau_{ij}}{\partial x_j} \tag{1}$$

where $\bar{u}_j$ and p are filtered mean velocity and filtered pressure, respectively. τ_{ij} is the subgrid-scale stress resulting from the filtering operation that is unknown and is modeled as

$$\tau_{ij} = -2\mu_t \bar{S}_{ij} + \frac{1}{3}\tau_{kk}\delta_{ij},\ \bar{S}_{ij} = \frac{1}{2}\left(\frac{\partial \bar{u}_i}{\partial x_j} + \frac{\partial \bar{u}_j}{\partial x_i}\right) \tag{2}$$

where μ_t is the subgrid-scale turbulent viscosity, and $\bar{S}_{ij}$ is the rate-of-strain tensor.

2.2. Smagorinsky-lilly model

The subgrid-scale turbulent viscosity (μ_t) is modeled using the Smagorinsky model, where the eddy viscosity is modeled as

$$\mu_t = \rho L_s^2 |\bar{S}| = \rho L_s \sqrt{2\bar{S}_{ij}\bar{S}_{ij}},\ L_s = \min(k\delta, C_s V^{1/3}) \tag{3}$$

where L_s is the mixing length for subgrid scales, k is the von Kármán constant, C_s is the Smagorinsky constant, δ is the distance to the closest wall, and V is the volume of the computational cell.

2.3. Description of grid domain

The geometries used in this study are elongated rectangular sections (i.e., width to depth ratio of 10 and 20), and a box girder bridge section with and without section details. The computational domain used for both steady and unsteady analyses is shown in Fig. 1, where the domain is divided into static and moving zones.

The width and depth of the domains are $105D$ and $60D$, respectively. A close-up of the mesh generated around the test sections is shown in Fig. 2. The corners of rectangular sections are considered rounded with a radius to depth ratio (r/D) of 0.01 and small size meshes are generated near each edge corner to avoid singularity of the solutions, and equally distributed 12 meshes were used in the span wise direction. The dimensions of model sections and analysis conditions used in this study are summarized in Table 1. Inflow wind velocity "U" is kept constant for any case to avoid any additional phenomenon, if any, arising with the change in Reynolds number (R_N). Also, throughout unsteady investigations, the angle of attack, i.e. the angle between the direction of width B and that of the uniform flow, was kept zero. The maximum intensity of turbulence is of the order of 0.001% at the inlet boundary. Symmetry condition was used for the top and bottom surfaces of the domain.

The steady aerodynamic coefficients of the streamline box girder bridge section are investigated for both cases, with and without section attachments like handrails, inspection rails, central barrier, etc. To include these attachments, a schematic use of structured/unstructured grid is introduced around the complex geometry (see Fig. 2b). First, the domain of interest is divided into two parts where regions away from the section are modeled using a structured grid, and the domain near and around the complex geometry is further divided into sub-domains. Within these sub-domains, which contain small

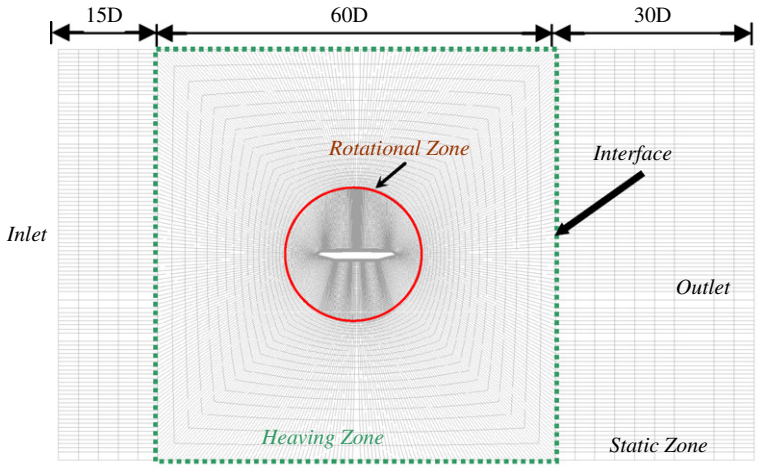

Fig. 1. Computational domain for steady and unsteady cases.

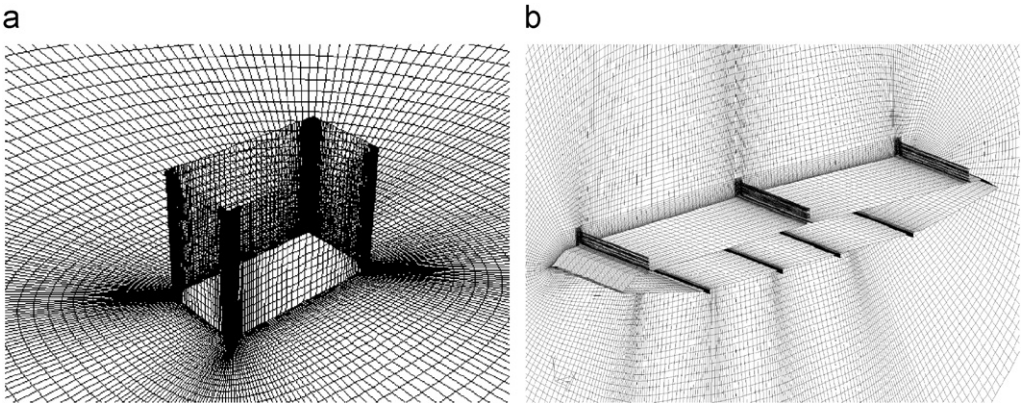

Fig. 2. Domain in vicinity of test sections: (a) rectangular section and (b) box girder section.

Table 1
Analysis conditions for rectangular prisms and box girder bridge section

	Symbol	Units	Rectangular prisms		Box girder section
Width	B	(m)	0.1	0.2	0.14864
Depth	D	(m)	0.01	0.01	0.0128
Spanwise length	$L(=3D)$	(m)	0.03	0.03	0.0384
Width to depth ratio	B/D		10	20	11.6125
Reynolds number	R_N		1.3×10^4	1.3×10^4	1.0×10^4
Wind velocity	U	(m/s)	20	20	14
Scale					1/250
Wind word front area	$A=LD$	(m^2)	0.0001	0.0001	4.9152E−04
Number of nodes			439,000	448,000	466,908
Non-dim time step (steady)	$\Delta\tau$		0.04	0.04	0.04
Non-dim time step (unsteady)	$\Delta\tau$		0.15	0.15	0.12

attachments, all quantities substantially vary near the solid boundaries and accuracy is especially important. Therefore, tetrahedral grids are employed to ensure a sufficient number of grids (see Fig. 3).

For unsteady analysis, the model sections are subjected to forced oscillations in the heaving and torsional modes, and the sliding mesh technique with the non-periodic velocity-inlet grid interface is employed to allow the forced oscillations in the heaving and torsional modes (FLUENT, 2005). The boundary conditions for the wall zones produced from the moving interface zones are set to velocity-inlet in order to keep uniformity of flow near the outer edges of the simulated domain. The reduced velocity of flow is changed by changing the frequency of forced vibration, rather than changing the velocity of wind flow, which is a usual way in wind tunnel experiments. For each model, equally spaced seven cases with reduced velocity ranging from 3 to 21 were chosen for the investigation purposes.

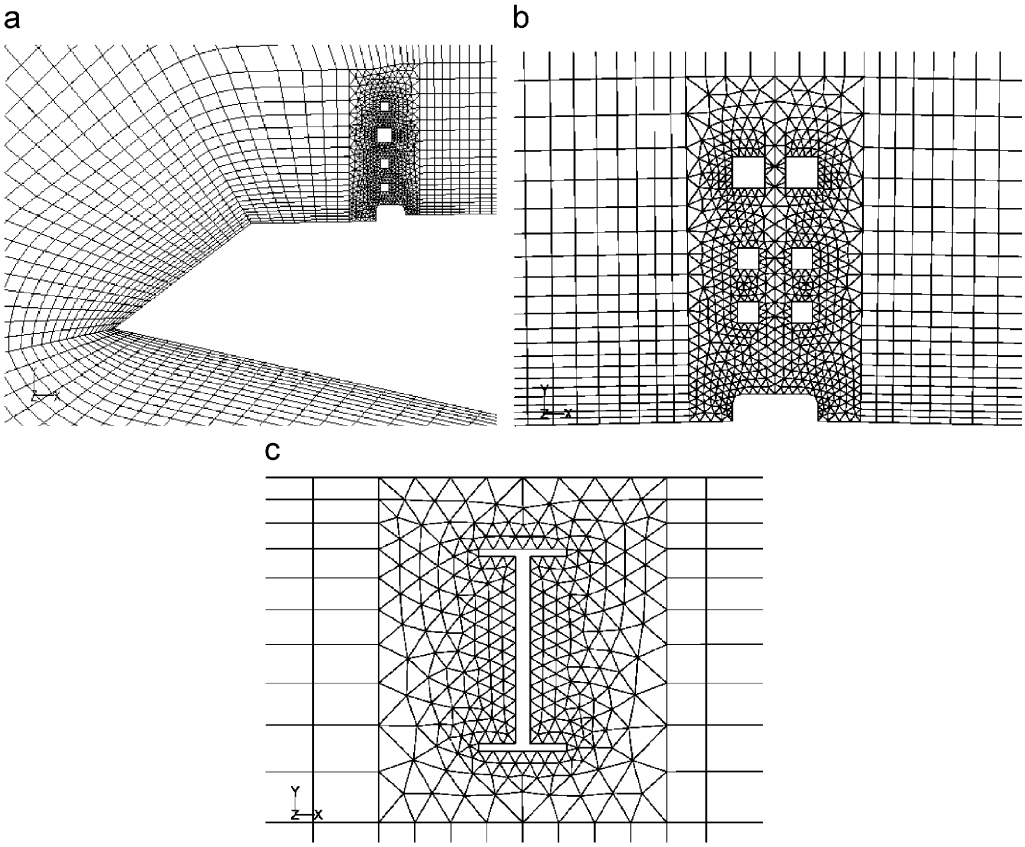

Fig. 3. Details of mesh generation around the section attachments: (a) Upwind handrails; (b) Central barrier and (c) inspection rails.

3. Modeling details and aerodynamic coefficients

This section includes the discussion based on steady investigations to determine the influence of geometrical modifications and section details on the aerodynamic characteristics. Further, modification in flow field around the streamline section due to the section attachments is examined.

3.1. Reynolds dependency of aerodynamic coefficients

Definition of the forces acting on model sections and the angle of attack along with displacement are shown in Fig. 4. Definition of mean aerodynamic force coefficients is summarized below:

$$C_D = \frac{F_D}{1/2\rho U^2 DL} \tag{4}$$

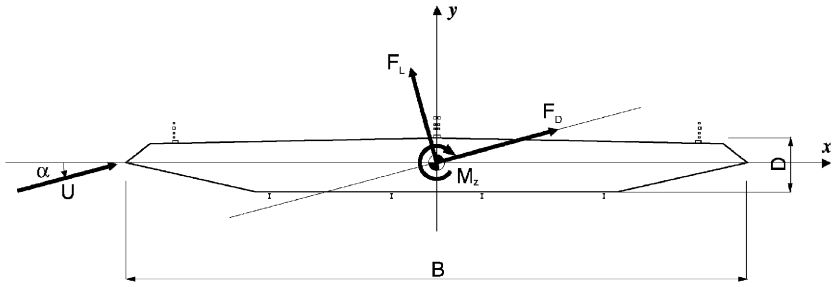

Fig. 4. Positive definitions of global forces and angle of attack.

$$C_L = \frac{F_L}{1/2\rho U^2 BL} \tag{5}$$

$$C_M = \frac{F_M}{1/2\rho U^2 B^2 L}. \tag{6}$$

An experimental Reynolds number (R_N) dependency study for the box girder section was conducted for both cases, with and without section attachments. The height of the model is chosen so that the blockage ratio remains below 3%. The details of the experiment performed to determine the steady aerodynamic coefficients are summarized in Ref. Ishihara et al. (2006b). The steady aerodynamic coefficients of sections with and without small attachments remain undisturbed with increase in Reynolds number. Since measurements at low wind velocity may strongly influence the accuracy of the results, Reynolds number was kept constant ($R_N = 3.5 \times 10^4$) throughout the experiments for both sections (i.e., with and without handrails and inspection rails). However, the numerical simulations are performed at a relatively low Reynolds number, i.e., $R_N = 1.0 \times 10^4$.

3.2. Coefficients of mean aerodynamic forces

Fig. 5 shows the dependence of mean aerodynamic coefficients on the angles of attack, ranging from -15° to $+15^\circ$, for the streamline box girder section with and without small attachments, using LES and κ–ε models.

In Fig. 5a, C_D attains the minimum value at about 0° and a moderate increase in C_D is observed in the range of $+7^\circ$ to -7°. Rather rapid increase in C_D is observed with further increase in the angle of attack for both cases. At a smaller angle of attack, the drag coefficient of the bridge section without attachments turns out to be one-third of the section with small attachments and also smaller than the rectangular sections, e.g., for $B/D = 20$–10, C_D ranges from 0.8 to 1.0, respectively. The use of the 2D standard κ–ε model overestimates the drag acting on the bridge section for both cases, whereas LES results show good agreement with those of the experimental ones. The contribution of each component of the bridge section is summarized in Fig. 6a. At 0°, the cumulative drag acting on handrails and inspection rails turns out to be larger than that acting on the bridge section only. At larger angles, most of the drag is contributed from the bridge section compared to the small attachments. For a positive large angle of attacks, the drag

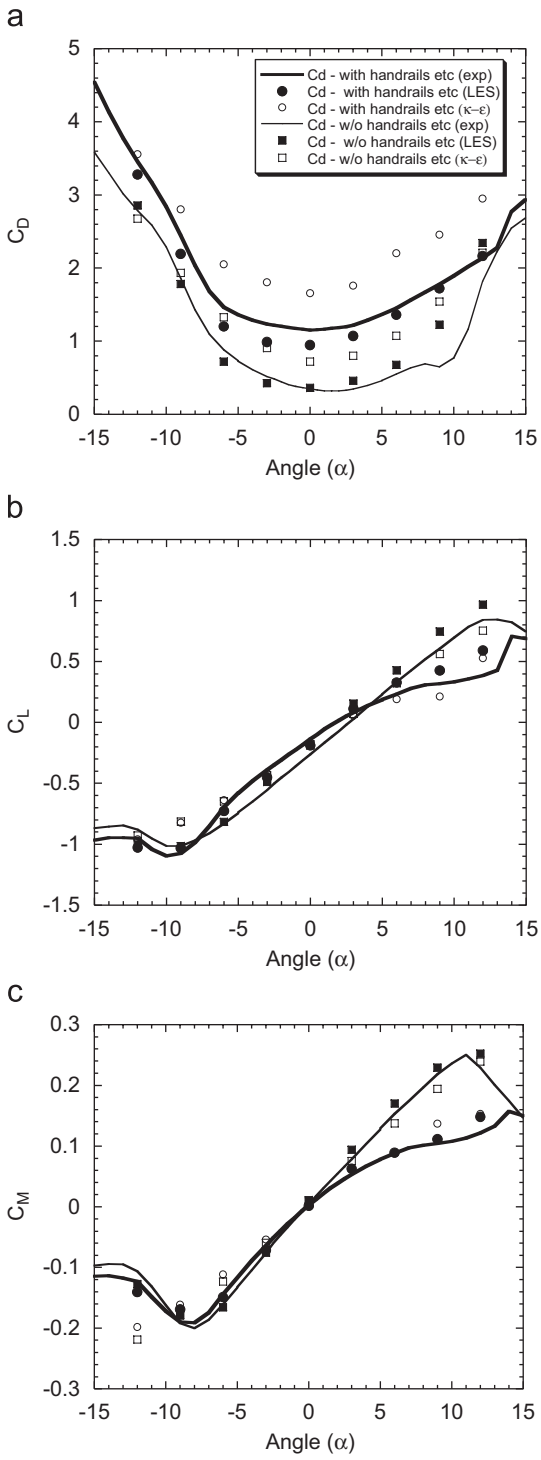

Fig. 5. Comparison of experimental and numerical aerodynamic coefficients of a box girder bridge section with and without handrails: (a) drag coefficient, (b) lift coefficient and (c) moment coefficient.

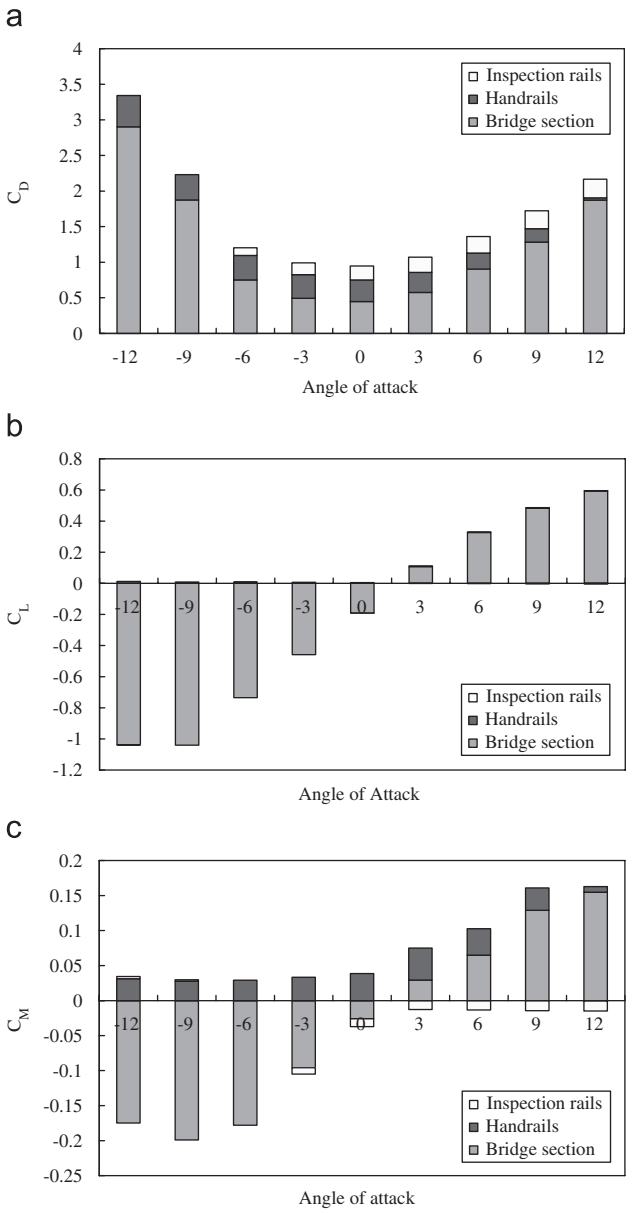

Fig. 6. Contribution of handrails and inspection rails to the aerodynamic coefficients of the bridge section by LES: (a) drag coefficient, (b) lift coefficient and (c) moment coefficient.

force acting on handrails reduces to zero at 12° and that on the inspection rails is doubled. However, for a negative angle of attacks, contribution of the drag from inspection rails is diminished and that from the handrails is increased.

The small section attachments do not significantly influence the lift force coefficient for negative attack angles, but the peak observed at the positive attack angle for the section

without attachments disappears in the presence of these attachments, whose mechanism will be explained in the next section. Also, the magnitude of lift force acting on hand and inspection rails becomes negligible, see Fig. 6b, and reduction in the lift force is mainly due to modification of the flow field around the bridge section by these attachments. In the absence of section attachments, the moment coefficient (C_M) increases naturally with an increase in attack angle and a maximum value occurs at about $+12^\circ$ and -9°. However, presence of small attachments has contained the moment at positive attack angles. Fig. 6c shows that, for a positive range of attack angles, the contribution of handrails to moment coefficients remains positive and inspection rails have shown negative contribution. Thus, inclusion of the small attachments may cause favorable or adverse influence on the aerodynamic characteristics of the bridge section, which will be discussed in the next section.

In short, the use of fairing to modify the rectangular sections reduces the drag force acting on the bridge section. However, the inclusion of small section attachments results in a higher drag force that depends on the size and density of these attachments. Thus, it shows the very importance of the modeling section details in order to obtain realistic aerodynamic behavior of the bridge sections.

3.3. Mean flow around the box girder bridge section

Looking at the flow field (Fig. 7) around the box girder section would help to identify the characteristics of mean force coefficients. Flow characteristics at three attack angles are discussed where large differences between aerodynamic coefficients of both bridge sections exist.

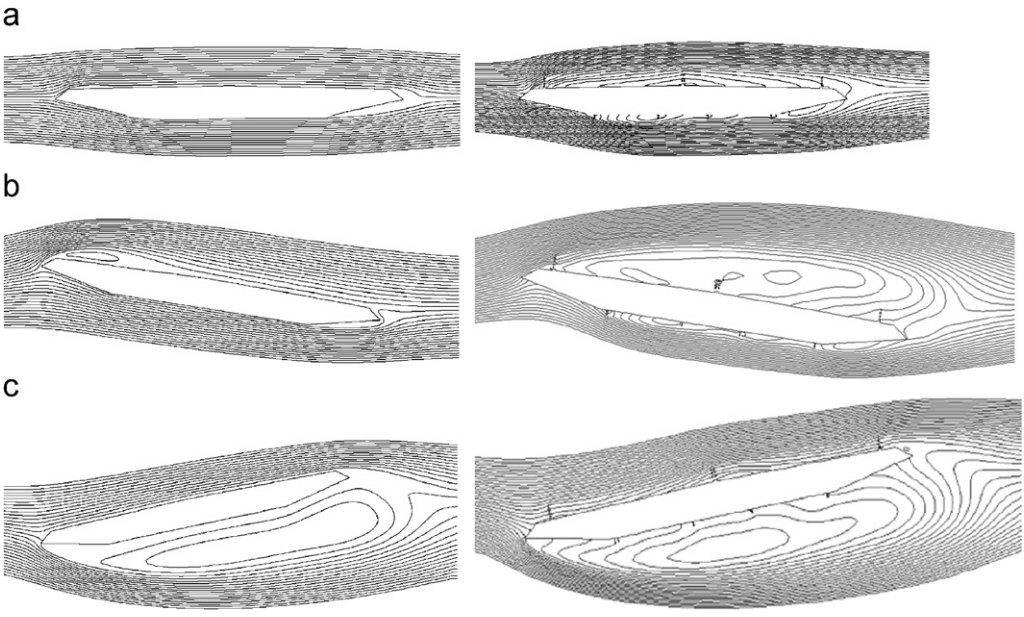

Fig. 7. Mean streamlines at different angle of attacks for the box girder bridge section without (left) and with (right) handrails. (a) $\alpha = 0^\circ$, (b) $\alpha = 9^\circ$ and (c) $\alpha = 12^\circ$.

At an attack angle of 0°, in case of section without attachments, the large positive pressure acting on fairing is followed by flow separation over a very small region on the windward side of the upper surface, as shown in Fig. 7a. The separated flow then reattaches to the upper surface and pressure recovery occurs. On the lower surface, separation of flow shows large negative pressure at the end of the lower flap, and the following reattachment of flow towards the leeward side indicates recovery of pressure on the lower surface of section (Fig. 7a).

In case of bridge section with attachments, at zero angle of attack, the flow is intercepted by the presence of handrails in addition to that acting on the upper flap surface. However, the flow along the upper surface remains separated and reattaches to the upper surface in the vicinity of leeward edge. On the other hand, the flow separation is intensified by the presence of a first handrail on the upper surface. The flow pattern around the section with attachments, as seen in Fig. 7a, shows that the flow separation on the lower surface caused by the first inspection rail reattaches between the 2nd and 3rd inspection rails. But next inspection rails again cause flow detachment. Thus, it shows the contribution of section details to the drag coefficient at 0°, as observed in Fig. 6a, which corresponds to the large drag force acting on the hand and inspection rails.

Fig. 7b shows the flow pattern around both sections at an attack angle of 9°. For the section without attachments, separation of flow on the upper surface intensifies and the length of separated flow increases with increase in the angle of attack, and flow reattaches to the upper surface near the mid of section width (Fig. 7b). On the lower surface, shear layers formed near the corners disappear by the time the angle changes to 9°. The negative pressure at the upper surface and positive pressure at the lower surface maximizes at this angle, and a large lift force is experienced by the bridge section as shown in the previous section. However, in case of section with attachments, flow separation intensifies on the windward side with an increase in the angle of attack and shows intermittent reattachment to the upper surface. At this angle, the windward handrails are still subjected to flow separating from the upper flange of fairing, and are contributing to the drag force. Also, increase in distance from the center of the bridge section results in large contribution to moment coefficient by the handrails. However, on the lower surface, flow reattaches in an intermittent fashion due to vortex formation behind the inspection rails. The negative pressure caused by separated flow thus results in a rather lower lift acting on the bridge section.

Fig. 7c shows the flow around both sections for a negative attack angle of 12°. On the upper surface of both sections, flow remains attached to the surface but all the handrails are exposed to a rather mild flow. Whereas on the lower surface, intensive negative pressure at the leading edge is improved by pressure recovery towards the leeward side in both cases, see Fig. 7c. The inspection rails come in wake of leading edge and do not influence the flow field that is observed in case of positive attack angles, see Fig. 7a, b. The difference in flow field around both sections remains quite minimal that results into almost similar force coefficients, which are found consistent with those of experimental values, as shown in Fig. 5.

4. Estimation of aerodynamic derivatives

In this study, the unsteady aerodynamic forces are simulated using the forced vertical and rotational excitations of a single degree of freedom system that are later used for

evaluating the aerodynamic derivatives. The force time histories obtained by forced vertical and rotational excitations are decomposed into components corresponding to the aerodynamic damping and stiffness by using Fourier decomposition (Washizu et al., 1978). Following the experiments by Matsumoto et al. (1994), in this study, the amplitudes of vibrations in heaving and torsional motions are kept as $y_0/B = 0.025$ and $\alpha_0 = 2^\circ$. Through measurement of the pressure distribution along periphery of sections, eight aerodynamic derivatives proposed by Scanlan and Tomko (1971) were obtained where unsteady lift (L) and pitching moment (M) are expressed as follows:

$$L = \frac{1}{2}\rho U^2(2b)\left[kH_1^*\frac{h}{U} + kH_2^*\frac{b\alpha}{U} + k^2H_3^*\alpha + k^2H_4^*\frac{h}{b}\right] \tag{7}$$

$$M = \frac{1}{2}\rho U^2(2b^2)\left[kA_1^*\frac{h}{U} + kA_2^*\frac{b\alpha}{U} + k^2A_3^*\alpha + k^2A_4^*\frac{h}{b}\right] \tag{8}$$

where $k = b\omega/U$, $B = 2b$ is the girder width, U is the mean wind velocity and ω is the bridge oscillating frequency in rad/s.

Experimental investigations of the same box girder section without section attachments were conducted by Zhu et al. (2006) to determine the influence of yaw angle on flutter characteristics. The dominant aerodynamic flutter derivatives of the box girder section without section attachments are shown in Fig. 8. The experimental flutter derivatives of the box girder section (Zhu et al., 2006) shows the tendency of A_2^* similar to that of the rectangular section $B/D = 20$. The simulated derivatives of the box girder section have shown good agreement with the experimental results, thus validating the accuracy of the LES model to examine the flutter characteristics of the box girder section.

Fig. 9 shows the simulated aerodynamic derivatives of rectangular sections with a width to depth ratio of 10 and 20 in comparison to those of the experimental results. The aerodynamic coefficients of the coupled derivative terms are found to be in good agreement with the experimental ones. However, predicted uncoupled terms for both

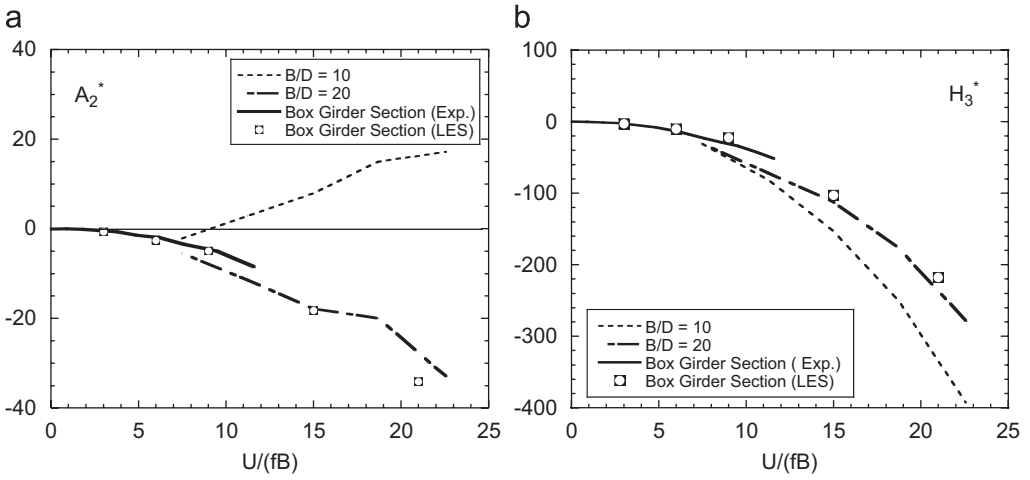

Fig. 8. Comparison of the simulated (LES) and experimental (Zhu et al., 2006) flutter derivatives for the box girder section, without handrails and inspection rails, along with rectangular sections (Matsumoto et al., 1994).

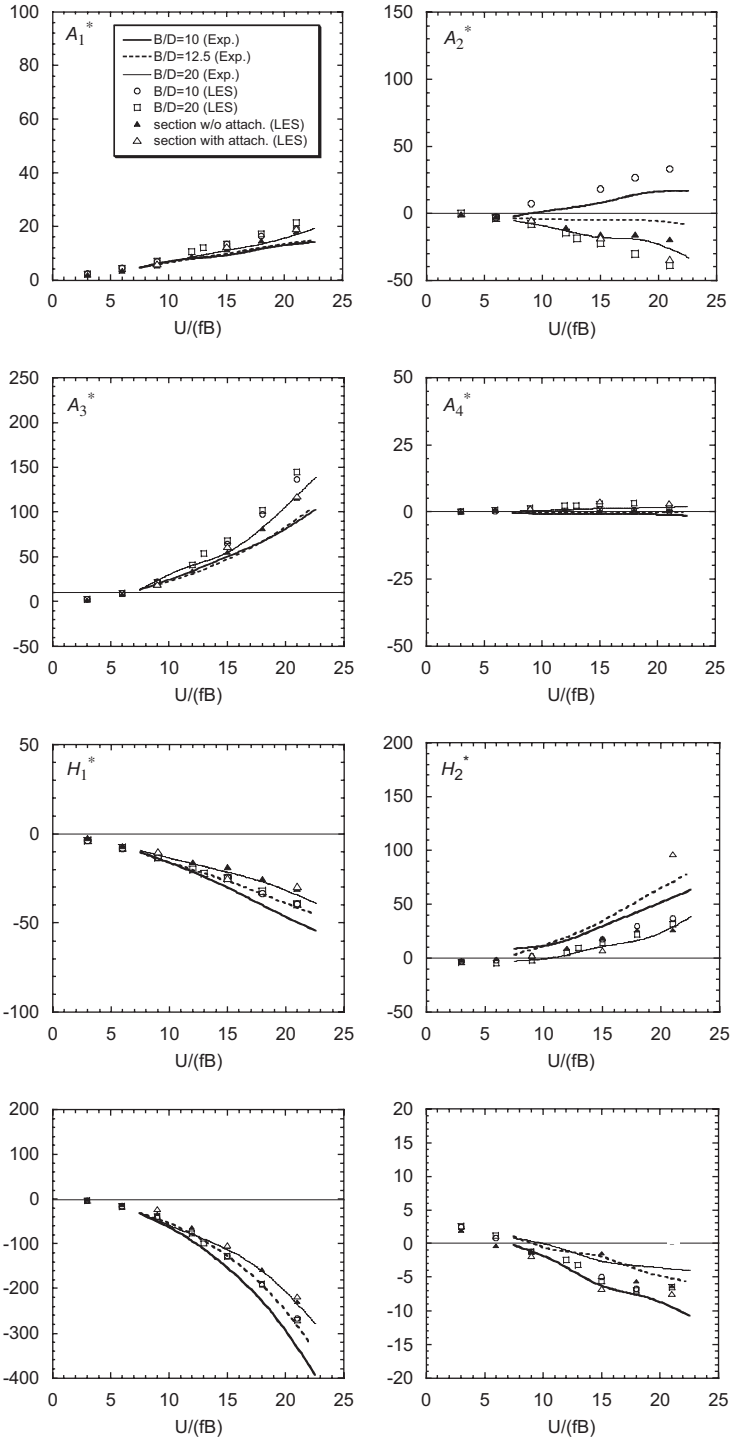

Fig. 9. Comparison of experimental (Matsumoto et al., 1994) and simulated flutter derivatives of rectangular sections, and those of box girder bridge sections, with and without small attachments.

sections turn out to be similar. This is due to small amplitudes of vibrations used in heaving and torsional modes to evaluate the unsteady aerodynamic derivatives. It could also be seen from the steady aerodynamic coefficients at small attack angles, which are similar for both rectangular sections. Since uncoupled terms are known to have less contribution to the flutter characteristics, flutter characteristics of the box girder bridge section are pursued.

The simulated flutter derivatives of the bridge section with small attachments ($B/D = 11.6$) show a close resemblance to those of the rectangular section with a higher width to depth ratio, i.e. 20, than the rectangular section of similar aspect ratio of 10, as shown in Fig. 9. This shows the dominant influence of the fairings used to obtain a bridge girder section that has limited separation of the shear layer and rather earlier reattachment of flow occurs. A good agreement is found among the aerodynamic derivatives of the bridge section and those of the elongated rectangular section with $B/D = 20$. To clarify the effect of hand and inspection rails, unsteady aerodynamic force coefficients of the bridge section without handrails are included at few reduced velocities and simulated flutter derivatives are summarized in Fig. 9. The moment derivative terms are found undisturbed by the introduction of small section attachments. However, the flutter derivatives corresponding to heaving of sections show rather large differences as shown in Fig. 9. This behavior of sections can be attributed to the difference observed for the static lift coefficients at the low angle of attacks, refer to Fig. 5b.

5. Flutter characteristics

Complex eigen value analysis, proposed by Miyata and Yamada (1990), is used to determine the circular frequency and logarithmic damping for heaving and torsional branches using the flutter derivatives obtained in the last section. Figs. 10 and 11 show the flutter frequency and the flutter damping ratio of rectangular sections with aspect ratios of 10 and 20, respectively. In Fig. 10a, it is obvious that the frequencies of two branches neck down near the reduced velocity corresponding to the critical flutter velocity, and again

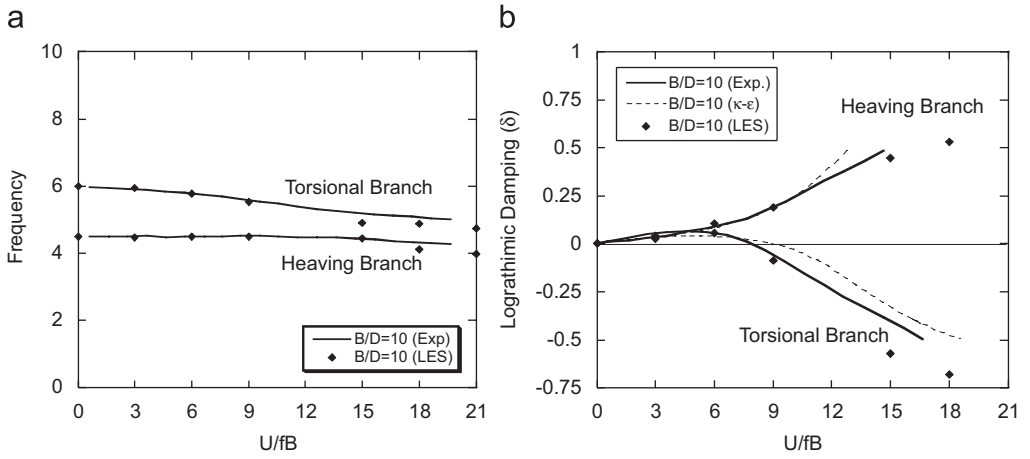

Fig. 10. Eigen value loci of rectangular section with $B/D = 10$ (experiment, κ-ε), $M = 1.96\,\mathrm{kg/m}$, $I = 4.9 \times 10^{-3}\,\mathrm{Kgm}$, $f_{\eta 0} = 4.5\,\mathrm{Hz}$, $f_{\omega 0} = 6.0\,\mathrm{Hz}$, $B(=2b) = 0.15\,\mathrm{m}$.

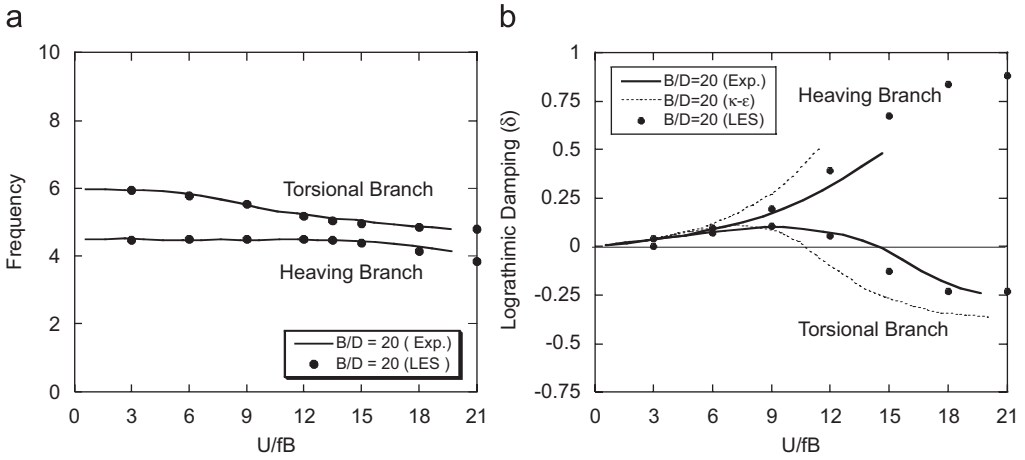

Fig. 11. Eigen value loci of rectangular sections with $B/D = 20$ (experiment, κ-ε) $M = 1.96\,\mathrm{kg/m}$, $I = 4.9 \times 10^{-3}\,\mathrm{Kgm}$, $f_{\eta 0} = 4.5\,\mathrm{Hz}$, $f_{\omega 0} = 6.0\,\mathrm{Hz}$, $B(=2\mathrm{b}) = 0.15\,\mathrm{m}$.

tends to part from each other at higher velocities. In case of flutter damping ratio, LES simulation shows increase in positive heaving branch and the damping ratio corresponding to the torsional mode changes from positive to negative at a reduced velocity of 9 (Fig. 10b). This indicates the possibility of torsional-type flutter at a reduced velocity, which is close to the critical flutter velocity of the section with $B/D = 10$ as reported by previous experimental study (Matsumoto et al., 1994). The logarithmic damping of both heaving and torsional branches is found to be in good agreement with experimental results (see Fig. 10b).

In case of rectangular section with an aspect ratio of 20, see Fig. 11a, flutter frequencies of two branches neck down near the reduced velocity of 13, which corresponds to the critical flutter velocity, and again tends to part from each other at higher reduced velocities. In case of flutter damping ratio, LES simulation shows an increase in positive heaving branch and the damping ratio corresponding to torsional mode changes from positive to negative at a reduced velocity of 13 (Fig. 11b). This indicates the possibility of torsional-type flutter at the intersection-reduced velocity, which is close to the critical flutter velocity identified by previous experimental study (Matsumoto et al., 1994).

It is noteworthy to mention here the work reported by Shimada et al. (2002), where the κ–ε model has shown conservative results for rectangular sections of similar aspect ratio, Figs. 10 and 11. This discrepancy in the identified flutter critical velocity was found due to the inaccurate prediction of aerodynamic coefficients A_1^* and H_3^*. On the other hand, LES has shown better prediction of such aerodynamic derivatives. Thus, it shows the effectiveness of 3D LES over a 2D κ–ε model to predict the flutter characteristics.

In case of streamline bridge section with an aspect ratio of 11.6, calculated heaving and torsional frequencies lead to torsional-branch coupled flutter type that coincides with the flutter characteristics of a rectangular prism with an aspect ratio of 20 (Fig. 12a). The logarithmic damping of the heaving branch remains positive for box girder sections with small attachments (Fig. 12b). However, logarithmic damping of the torsional branch becomes negative at high reduced velocity of 13 which is similar to that of the rectangular section with $B/D = 20$. The box girder section ($B/D = 11.6$) has shown higher critical

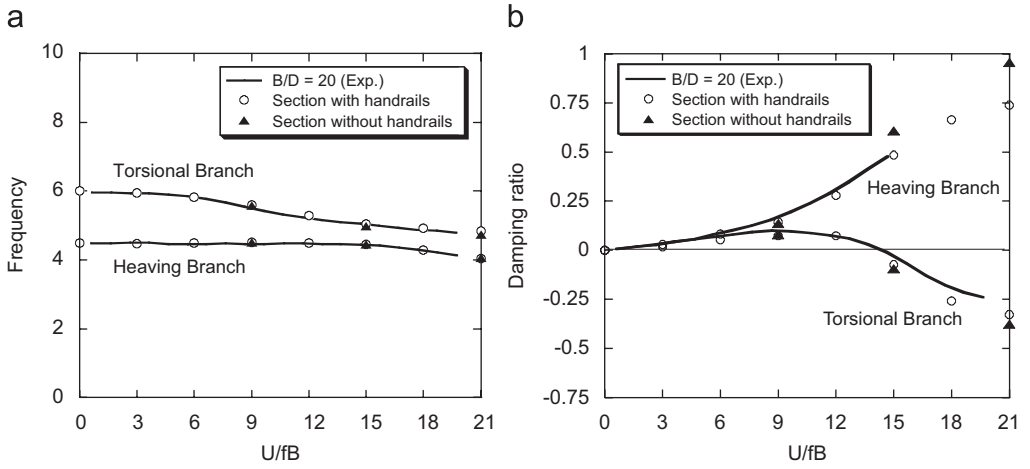

Fig. 12. Comparison of eigen value loci of the box girder bridge section with and without attachments along with the rectangular section ($B/D = 20$). $M = 1.96\,\mathrm{kg/m}$, $I = 4.9 \times 10^{-3}\,\mathrm{Kgm}$, $f_{\eta 0} = 4.5\,\mathrm{Hz}$, $f_{\omega 0} = 6.0\,\mathrm{Hz}$, $B(=2\mathrm{b}) = 0.15\,\mathrm{m}$.

flutter velocity than that of the rectangular section with a similar aspect ratio of 10. The flutter derivative A_2^* plays an important role in torsional stability and is sensitively influenced by changes in the geometrical shape of the bluff body (Matsumoto, 1996). This predominant aerodynamic coefficient, A_2^*, of the bridge section, which is obtained using fairings, turns out to be similar to those of the section with $B/D = 20$ than the section with $B/D = 10$. Thus, use of fairing in the bridge section with a smaller aspect ratio results in flutter characteristics equivalent to those of the section with a higher aspect ratio of 20.

To investigate the influence of section attachments, the flutter characteristics were calculated at selected reduced velocities of 9, 15 and 21. The flutter frequency and damping ratios for this case are also summarized in Fig. 12. The flutter characteristics remain undisturbed except for the damping of heaving branch, which becomes higher at higher reduced velocity. In the previous section, it was already shown that the dominant flutter derivatives remain unchanged in the absence of section attachments. This inability of showing the effect of section attachments may be due to two reasons. First, the amplitude of vibrations used for determining the unsteady characteristics was so small that it could not include the influence of these attachments on unsteady aerodynamic characteristics. It can be clarified by seeing the static aerodynamic coefficients, see Fig. 5, that were found to be almost similar for both cases, i.e., section with and without attachments, at a smaller angle of attack. Secondly, these attachments were placed behind the separation point at the leading edge and the density of handrails is so minimal that the presence of section details did not show a strong impact on aerodynamic characteristics of the bridge section.

6. Conclusion

Sections details are found to have a strong influence on the steady aerodynamic coefficients that result in a higher drag coefficient at low angles of attacks, whereas lift and moment coefficients are reduced at large angle of attacks. Therefore, modeling of section details is required to simulate the realistic characteristics of bridge sections. The unsteady

characteristics of an elongated rectangular section, simulated by the LES turbulence model, are found to be in good agreement with the experimental results. Further, the effectiveness of the 3D LES model over the 2D κ–ε model in predicting the steady force coefficients and the flutter characteristics is shown. Use of fairing to obtain streamline bridge section has strongly affected the flutter derivative A_2^*, which is sensitive to the shape of the section. The flutter characteristics of the streamlined bridge section ($B/D = 11.6$) are found to be closer to the rectangular section with of high aspect ratio, i.e., 20 than that of 10. This indicates that the use of fairing, to achieve a section with higher critical velocity and smaller aspect ratio, is a suitable option that results in A_2^* corresponding to high flutter critical velocity. This study thus concludes that the LES turbulence model is an effective technique for estimating aerodynamic characteristics of the complex geometrical sections.

References

Bruno, L., Khris, S., Marcillat, J., 1998. Contribution of numerical simulation to evaluating the effect of section details on the aerodynamic behavior of a long-span bridge deck. Wind Engineering into the 21st Century, Larsen, Larose and Livessey, Balkema, pp. 1229–1236.

FLUENT 6.2.16, 2005. User's Guid, Fluent Incorporated.

Ishihara, T., Oka, S., Fujino, Y., 2006a. Numerical prediction of aerodynamic characteristics of rectangular prism under uniform flow. J. Struct. Earthquake Eng. 62A, 78–90 (in Japanese).

Ishihara, T., Shimada, K., Yamasaki, Y., Ikeda, T., 2006b. A study of aerodynamic characteristics of a cable stayed bridge girder by 3D numerical simulation. J. Struct. Eng. 52A JSCE.

Jones, N.P., Scanlan, R.H., et al., 1995. The effect of section model details on aeroelastic parameters. J. Wind Eng. Ind. Aerodyn. 54/55, 45–53.

Larsen, A., 2006. Computation of aerodynamic derivatives by various CFD techniques. In: The Fourth International Symposium on Computational Wind Engineering, Yokohama, Japan, pp. 287–290.

Larsen, A., Walther, J., 1998. Discrete vortex simulation of flow around five generic bridge deck sections. J. Wind Eng. Ind. Aerodyn. 77–78, 591–602.

Matsumoto, M., 1996. Aerodynamic damping of prisms. J. Wind Eng. Ind. Aerodyn. 59, 159–179.

Matsumoto, M., Niihara, Y., Kobayashi, Y., 1994. On the mechanism of flutter phenomena for structural sections. J. Struct. Eng. 40A, 1019–1024 (in Japanese).

Matsumoto, M., Kobayashi, Y., Shirato, H., 1996. The influence of aerodynamic derivatives on flutter. J. Wind Eng. Ind. Aerodyn. 60, 227–239.

Miyata, T., Yamada, H., 1990. Coupled flutter estimation of a suspension bridge. J. Wind Eng. Ind. Aerodyn. 33, 341–348.

Scanlan, R.H., Tomko, J.J., 1971. Airfoil and bridge deck flutter derivatives. J. Mech. Div. 97, 1717–1737 ASCE.

Shimada, K., Ishihara, T., Wakahara, T., 2002. Prediction of flutter characteristics of rectangular cross-sections by κ–ε model. In: The Second International Symposium on Wind and Structures, pp. 211–218.

Washizu, K., Ohya, A., Otsuki, Y., Fuji, K., 1978. Aeroelastic instability of rectangular cylinders in a heaving mode. J. Sound Vib. 59 (2), 195–210.

Zhu, L., Chang, G., Li, C., 2006. Skew wind effect on 2-DOF coupled flutter of a flat-box deck. In: The Fourth International Symposium on Computational Wind Engineering (CWE2006), Yokohama, Japan, pp. 497–500.